3D ACOUSTICAL CHARACTERIZATION OF AN ELECTRICAL MOTOR BY BAYESIAN FOCUSING

Thibaut Le Magueresse[1], Allan Outrequin[1], Michael Thivant[1], Jérôme Antoni[2], Jean-Louis Jouvray[3] and Etienne Robert[3]
[1]MicrodB
28 chemin du petit bois, 69131 Ecully, France
[2] Univ Lyon, INSA-Lyon, Laboratoire Vibrations Acoustique
[3]Groupe Renault

ABSTRACT

The industrial sound characterization of noisy objects by imaging techniques is subject to practical constraints (limitations of the number of arrays, restriction of the acquisition duration, noisy environment) and the characterization itself is challenging (3D description of the field in terms of directivity or absolute acoustic sound power per component for example). Therefore, the use of advanced imaging techniques such as three-dimensional inverse methods becomes relevant. The present study aims at illustrating advantages of the Bayesian Focusing through a deep analysis of the radiation of an electrical motor mounted on a test bench. First the importance of modelling realistic acoustical transfer functions will be highlighted. Then, the wealth of information given by the method in terms of source description will be illustrated. The robustness with respect to the number of snapshots will be studied. Finally the quality of reconstruction may be estimated by computing statistical criteria.

1 INTRODUCTION

The paper presents some results extracted from a larger study which aimed at characterizing the radiation of an electric motor used for the hybridization of a conventional motor. The electric machine is mounted on the gearbox and is able to provide power according to driving conditions. The particular interest concerns the radiation of the 48th motor order, for which a problematic acoustic behaviour had been identified. In order to treat the motor efficiently, satisfying mass and cost constraints, it has been proposed to apply imaging techniques to localize and quantify the sound sources appearing on the motor. Both the small dimensions of the motor and the expectations in terms of spatial resolution imply to perform a measurement in the nearfield of the motor. Moreover, the spatial complexity of the object of interest must be respected to precisely identify location of the sources. The solution adopted is a 3D imaging method taking into account both correlation relationship between sources and their scattering effect on the surface of the motor. Therefore, deconvolution methods are not in the scope of

this study since they aim at reconstructing uncorrelated sources [1]. Instead, methods falling within the category of 3D inverse methods could be suited for this problematic. Methods based on a propagation models computed from integral formulation may be applied (inverse Boundary Element Method [2], inverse Patch Transfer Functions [3]). Computation time and data setting for the calculation of the propagation model presents the major difficulties of these approach for an efficient industrial application. Methods based on representing the field as superposition of virtual sources are also subject to an extensive literature [4], [5], [6], [7]. However, the scattering effect are generally not considered in these approaches unless transfer functions are computed by FEM [8] or measured [9], which presents the disadvantage of long implementation time mentioned above.

In that context, Bayesian focusing [10] presents the characteristic to unify some of the aforementioned methods by formulating the inverse problem with the Bayesian formalism. Playing with prior knowledge about the source or the noise may obtain results similar to those obtained with beamforming or Near Field Acoustic Holography, for example [11]. Spatial resolution and quantification performances may both be improved compared to classical Tikhonov approach, by introducing sparsity enforcing priors though the statistical modelling of the sources [12]. Moreover, this method is flexible enough to automatically and robustly set the regularization parameter [13] and takes as an input data the Cross-Spectral Matrix (CSM) of array measurements [12]. Finally, performances of the method can be quantitatively evaluated by mapping uncertainties involved by experimental uncertainties or by the algorithm itself [14].

Bayesian focusing takes as input data (a) prior knowledge about the sources and noise, (b) measured data and (c) deterministic propagation model between the potential sources and the microphones array. Meanwhile, a recent sensitivity analysis of the method reveals that the main source of uncertainty comes from propagation model errors [15]. Therefore, it seems to be essential to couple the method with more realistic transfer functions than the free-field assumption commonly made. In this paper, Equivalent Source Method (ESM) [16] is proposed to compute with reasonable computation cost the acoustical transfer functions by modelling a scattering boundary conditions on the skin of the object.

The objective of this paper is to apply the Bayesian Focusing method together with a propagation model calculated by ESM on an industrial application. First, the case study will be described. Then, the theoretical aspects of the Bayesian focusing method and ESM will be recalled. The influence of the use of a refined transfer function on the imaging results and the robustness of the Bayesian focusing with regards to the convergence of the CSM will be studied. Finally, the fidelity of the reconstructed sources in terms of directivity will be experimentally assessed.

2 DESCRIPTION OF THE EXPERIMENTAL SET-UP

The motor is mounted on a specific test bench build by Vibratec. The study consists in investigating the radiation of an electrical motor provided by Groupe Renault and composed of a wound stator of 24 teeth and a rotor of 8 pairs of poles. The motor is remote-controlled by imposing the torque. It is connected to a second motor that plays the role of brake. The required speed is obtained by the value of the load imposed by this second motor. Since the purpose of the study is the characterization of the electrical motor, the other secondary acoustical sources have been treated by acoustical foam. The second motor has been encapsulated in a rigid box, as shown in Figure 1.

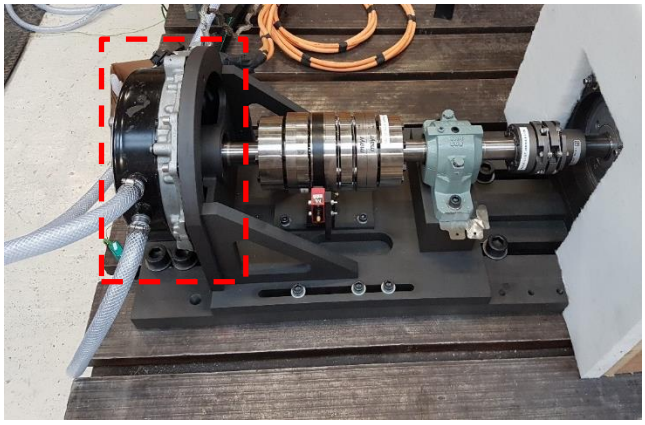

Figure 1: photography of the electrical motor (on the left, surrounded in red dotted rectangle) the shaft and a part of the second motor (on the right).

Two planar Simcenter HD acoustic cameras composed of 36 and 54 analog microphones have been placed in the nearfield of the motor to ensure the best coverage of the space. Their signals are simultaneously acquired by one single acquisition front end. The electrical bench has been digitized by the use of a Kinect optical sensor and the arrays have been positioned in the coordinate system of the mesh by triangulation. The photography of the bench with the arrays and the digitalized set-up are shown in Figure 2. During the study, a lot of operating points have been analysed. For this communication, only three among them will be shown: two stabilized operating points (speed of 1440rpm with 150Nm torque and 3940rpm with 80Nm) and one run-up (from 500 to 4500rpm with 80Nm torque).

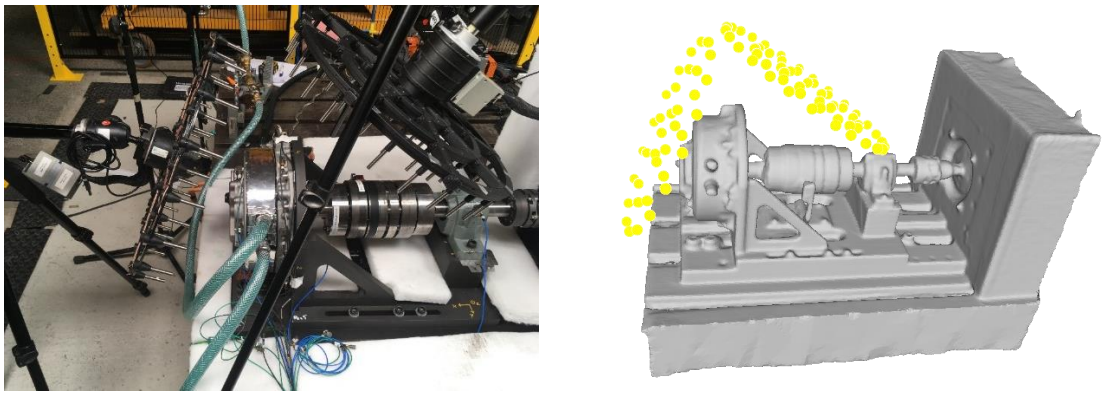

(a) (b)

Figure 2: photography of the experimental bench (a) and corresponding numerical set-up (b). In yellow, position of the microphones used for the back-propagation.

3 THEORETICAL ASPECTS

3.1 Iterative Bayesian focusing (iBf)

3.1.1 Forward problem

Once the geometry has been described and the CSM has been measured, sources may be reconstructed by solving the inverse problem. The corresponding forward problem is written as a linear matrix form, at a given frequency considering the i^{th} single temporal snapshot:

$$\mathbf{p}_i = \mathbf{G}\mathbf{q}_i + \mathbf{n}_i, \quad (1)$$

with $\mathbf{p}$ the complex amplitudes of the measured sound pressure stacked in a vector of dimensions of $[M\text{x}1]$ with M the number of microphones, $\mathbf{q}$ the vector of the source amplitudes of dimensions of $[N\text{x}1]$ with N the number of sources and $\mathbf{G}$ the matrix of dimensions of $[M\text{x}N]$ containing transfer function elements. Finally, the quantity $\mathbf{n}$ represents the additive noise applied on each microphone. The source field may be decomposed on spatial basis functions in order to unify several well-known methods [10]. In the present communication, the sources are modelled as virtual point sources placed on each node of the mesh. They are characterized by their volume velocity which has to be estimated using inverse method. The real source field is assumed to be represented by a distribution of discrete sources placed on the skin of the object. Then, the propagation matrix could be predicted by the free field analytical expression:

$$\mathbf{G} = -\frac{\mathrm{i}\omega\rho \mathrm{e}^{\mathrm{j}k\mathbf{R}}}{4\pi\mathbf{R}}, \quad (2)$$

with $\boldsymbol{R}$ the matrix of distances between the microphones and nodes. As shown in section 2, the study case involves nearfield measurement where microphones are subject to masking effect of sources induced by the presence of the motor. It may be relevant to take into account this effect. In that paper, ESM has been used to predict these scattering effects (see section 3.2).

3.1.2 Prior assumptions

Statistically, the noise distribution is assumed to follow a centred normal distribution governed by the Central Limit theorem [17]. Its covariance matrix, denoted $\boldsymbol{\Omega}_n$, is diagonal since the noise is assumed uncorrelated between sensors. Moreover, each microphone is noised in the same way; then the covariance matrix is equal the identity matrix $\boldsymbol{\Omega}_n = I$. Therefore the likelihood function follows a normal distribution as well, uncentered by the evaluation of the quantity $\mathbf{Gq}$. Finally, the choice of the prior probability density function concerning the sources modelling is large. It defines the statistical behaviour of the complex source amplitudes before measuring their radiation by the array. This question has been addressed to an entire paper [12]. The first prior which can be intuitively introduced is the notion of spatial aperture function: sources are more likely localized on the motor rather than situated on the bench support. Then it may be judicious to define spatial weights which could guide the algorithm. This spatial aperture may be automatically initialized by using beamforming approach for example. The principle of iterated Bayesian focusing resides in updating this aperture function iteratively to progressively add a spatial sparsity prior information. It has been shown that this aperture function may be modelled as a random quantity jointly estimated with the sources [12]. The aperture may be modelled by a probability density function which parametrizes the amount of sparsity. In the present communication, the Generalized multivariate complex Gaussian prior has been chosen with a norm p=1.3. It has been experienced that this choice is a convenient compromise between a high degree of sparsity (given by the Student law for example, or a smaller value of the norm p) and a low degree of sparsity given by the classical Tikhonov-form solution [12].

This large list of assumptions may be mathematically modelled by the Bayesian formalism. The elegance of the method resides in the explicit mathematical description of the whole physical assumptions that the user makes.

3.1.3 Solution

The solution is found by maximizing the posterior density function proportional to the product of the likelihood function and the prior distribution. The solution involves an iterative mechanism which automatically tunes the aperture function:

$$\widehat{\boldsymbol{q}}_{[\mathrm{k}]i} = \boldsymbol{\Sigma}_k^2 \boldsymbol{G}^H \left(\boldsymbol{G}\boldsymbol{\Sigma}_{[k]}^2 \boldsymbol{G}^H + \eta_{[k]}^2 \boldsymbol{I}\right)^{-1} \boldsymbol{p}_i, \tag{3}$$

with k the current iteration index, η^2 the regularization parameter and $\boldsymbol{\Sigma}_k^2$ a diagonal matrix containing the values of the aperture function at each node of the mesh. These two last quantities depend on the CSM of the sources $\widehat{\boldsymbol{S}}_{qq}^{[k]} = \frac{1}{I}\sum_{i=1}^{I} \widehat{\boldsymbol{q}}_{[\mathrm{k}]i} \widehat{\boldsymbol{q}}_{[\mathrm{k}]i}^H$ and the CSM of the measured pressure $\boldsymbol{S}_{pp} = \frac{1}{I}\sum_{i=1}^{I} \boldsymbol{p}_i \boldsymbol{p}_i^H$:

$$\boldsymbol{\Sigma}_k^2 = diag\left(\widehat{\boldsymbol{S}}_{qq}^{[k-1]}\right)^{1-\frac{p}{2}}, \text{ and} \tag{4}$$

$$\eta^2 = Argmax\left[\eta^2 \middle| \boldsymbol{S}_{pp}, \boldsymbol{\Sigma}_k^2\right]. \tag{5}$$

For further details about the calculation of the regularization parameter, interested readers can refer to [18]. Finally, the solution may also be expressed as a function of quadratic quantities:

$$\widehat{\boldsymbol{S}}_{qq}^{[k]} = \mathbf{G}_{\mathrm{inv}} \boldsymbol{S}_{pp} \mathbf{G}_{\mathrm{inv}}^H, \tag{6}$$

with $\mathbf{G}_{\mathrm{inv}} = \boldsymbol{\Sigma}_k^2 \boldsymbol{G}^H \left(\boldsymbol{G}\boldsymbol{\Sigma}_{[k]}^2 \boldsymbol{G}^H + \eta_{[k]}^2 \boldsymbol{I}\right)^{-1}$ is the inverse regularized kernel. In practice, the acoustic quantity of interest is the sound power that can be expressed from the volume velocity cross spectral matrix:

$$\boldsymbol{W}^{[k]} = \frac{\rho c k^2 diag\left(\widehat{\boldsymbol{S}}_{qq}^{[k]}\right)}{4\pi}. \tag{7}$$

As a remark, this expression describes the sound power of each equivalent source taken independently. Another expression can be used to model the interference created between the identified sources [19].

3.2 ESM-based propagation model

Since the motor is situated between the two arrays, its own presence will influence the propagation of waves measured by the arrays. This masking effect has to be implemented in the algorithm to avoid the reconstruction of ghost sources resulting a wrong representation of the propagation. The well-known ESM has been exploited to compute the transfer functions between the nodes of the potential sources and the microphones. The equivalent sources, arbitrary placed inside the motor, are calibrated in term of complex amplitude so that their radiation satisfies these following assumptions:

- The radiating object is rigid when the motor is switched off (normal velocity of nodes on the mesh is null);
- Sommerfeld radiation condition in the far field.

The method, initially developed as an alternative of Boundary Element Method (BEM) [16], has been customized to suit the imaging techniques needs [20] [21] [22]. For the present application, 1000 equivalent sources have been randomly placed inside the mesh as presented in Figure 3. The output of the ESM algorithm is the full propagation matrix $\boldsymbol{G}$ between the skin of the mesh and the microphone array in which scattering effect are modelled.

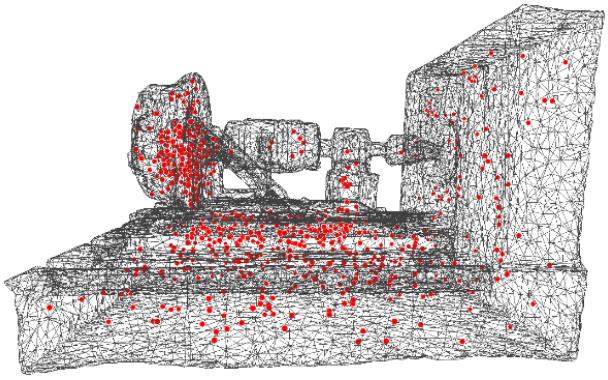

Figure 3: Mesh of the electrical bench (in gray) and equivalent sources positions (in red)

By way of illustration, the modulus of the pressure field generated by a point source placed at the position of one microphone of the array is displayed on Figure 4 (reciprocal transfer function). The sound field is propagated either using the free field (4a) or the ESM (4b). The masking effect is clearly modelled by ESM, whereas the free field propagation only described a decrease proportional to the propagation distance.

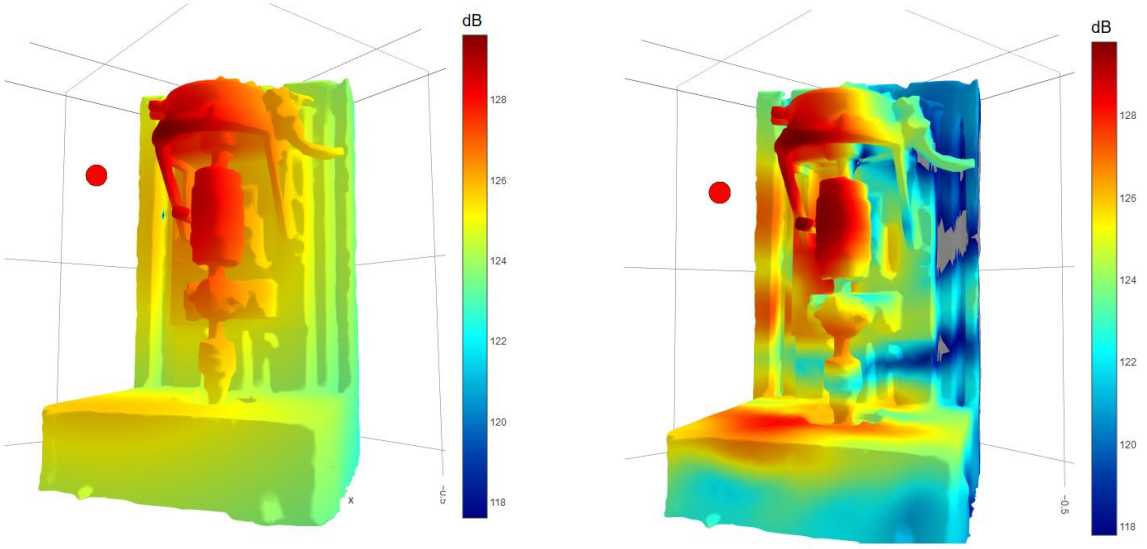

(a) (b)

Figure 4 : Sound pressure field on the skin of the object submitted to a unitary point source (represented in red) by assuming the free-field propagation (a) and by constraining the rigidity of the object using ESM (b) at 1150Hz.

The validation of the transfer function calculation based on ESM has been described in a recent paper [20].

4 POST PROCESSING: ITERATIVE BAYESIAN FOCUSING WITH ESM-BASED TRANSFER FUNCTIONS

4.1 Influence of the propagation model

The radiation of the e-motor has been recorded by the 90 synchronized microphones placed in the nearfield as shown in Figure 2. The motor was running with a torque of 150Nm at a speed of 1440rpm. iBf maps have been computed considering either free field or scattering assumptions. Figure 5 (a and b) shows the sound power maps obtained on the frequency range of [1-1.3]kHz corresponding to the 48th order at 1440rpm. With the free-field assumption, the main source is localized on the bracket of the bench, which may be interpreted as a mode shape of the bench. Applying iBf with ESM-based transfer function changes the interpretation of the results: the source apparently comes from the cover of the motor. In order to understand the real acoustical behaviour of the motor, an acoustic foam has been placed on this cover (see the photography of the Figure 5). The acquisition has been repeated on the same operating point. The results with the two models are shown on Figure 5 (c and d). It appears that the main source has been treated with the application of the foam. Then, in the situation in which the foam was not present, the real source was located on the cover and not on the bracket of the bench. In that case, the results given by iBf together with ESM transfer function is more reliable than the iBf with the free-field assumption.

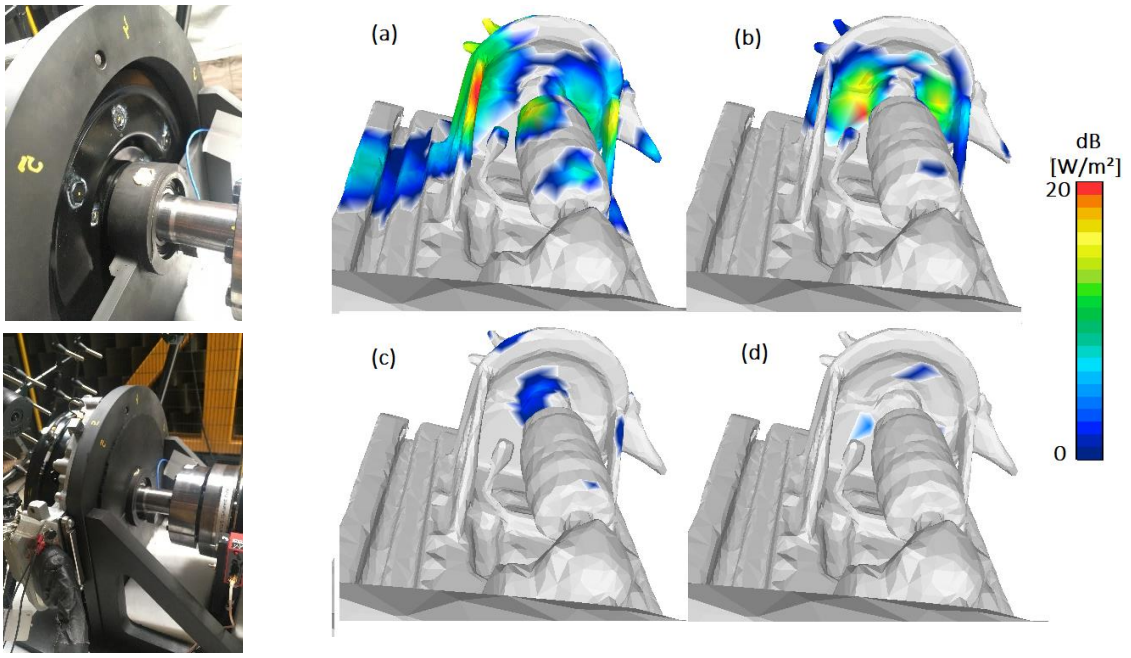

Figure 5 : Effect of the treatment of the cover applied on the motor: maps computed with free-field model (a and c) and with ESM (b and d) between 1kHz and 1.3kHz. The absolute values have been voluntarily masked for sake of confidentiality

Moreover, the origin of the radiation has been cross validated by an operating deflection shape which corroborate the results obtained by Bayesian Focusing using ESM propagation model.

4.2 Directivity of the sources

As the iBf provides the full cross-spectral matrix of the sources, it is possible to re-propagate these sources around the motor to assess their directivity:

$$|\hat{\boldsymbol{p}}|^2 = \mathrm{diag}\left(\boldsymbol{G}\,\hat{\boldsymbol{S}}_{qq}\;\boldsymbol{G}^H\right), \tag{8}$$

with $\boldsymbol{G}$ the ESM-based propagation matrix between the nodes of the mesh and the point where the directivity has to be computed, $\hat{\boldsymbol{S}}_{qq}$ the cross spectral matrix of the sources identified by iBf at the last iteration and $|\hat{\boldsymbol{p}}|^2$ the auto-spectrum of the virtual microphone placed where the directivity has to be computed. This process has been experimentally validated by placing the two arrays on the two sides of the motor, as presented in Figure 6. The signals have been recorded for the same operating point than above (1440rpm, 150Nm). The idea is to use these two additional positions of arrays as control arrays. The CSM of the sources estimated by iBf using the first two arrays (presented on Figure 2) have been re-propagated to the second two arrays placed on the sides of the motor (presented on Figure 6).

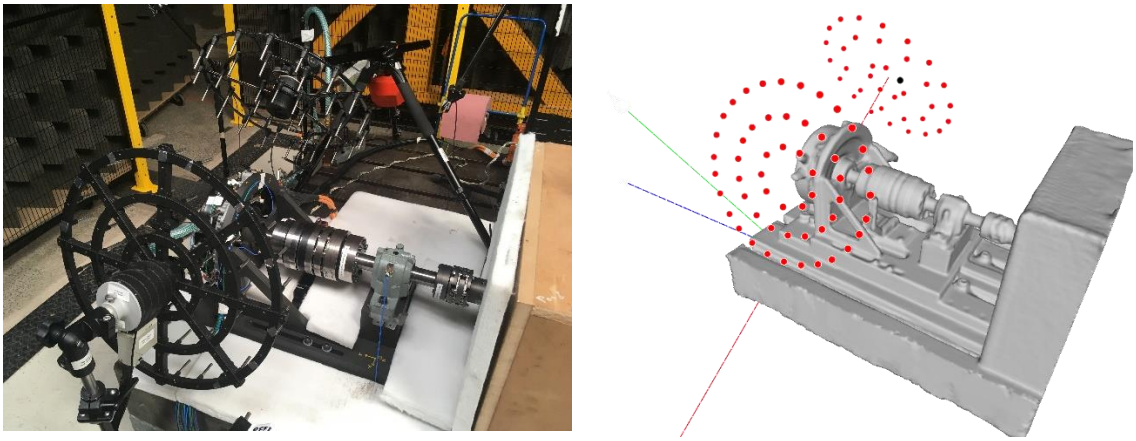

(a) (b)

Figure 6: Photography of the two control arrays (left) and numerical set-up (right). In red, microphones positions. In black, position of the control microphone on which the spectrum has been plotted on Figure 8

Figure 7 shows the measured and re-propagated pressure map at 1150Hz on the two control arrays. The re-propagation process predicts well the measured field.

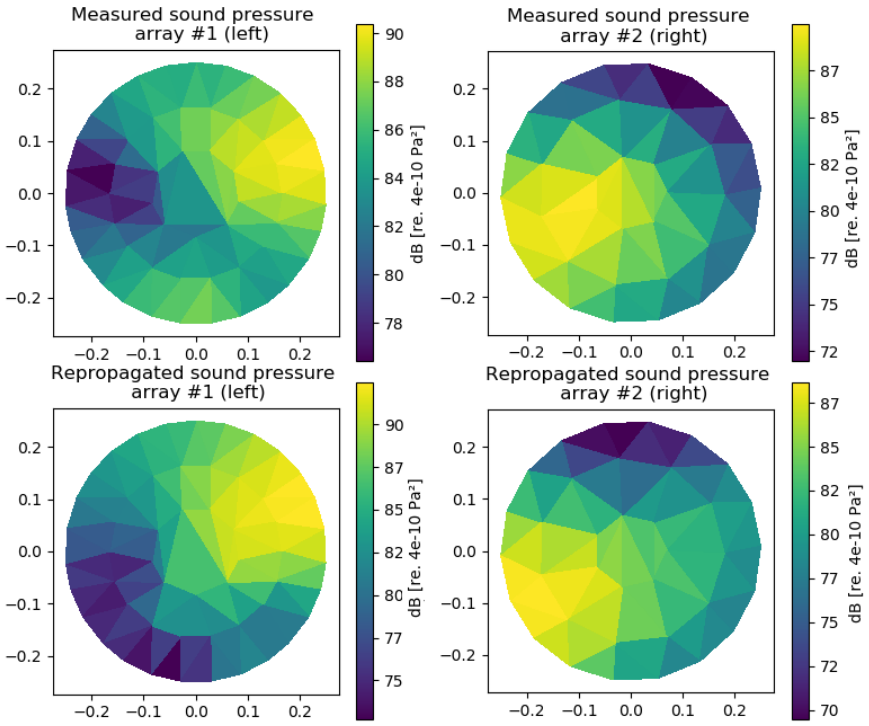

Figure 7: Measured (on the top, ground truth) and re-propagated (on the bottom) sound field for the left array (on the left) and the right array (on the right) at 1150Hz

The same post processing has been repeated for one control microphone (flagged in black on the Figure 6) as a function of the frequency. The Figure 8 shows both the measured and re-propagated autospectra of this microphone. The two curves fits well and indicates that the iBf respects the directivity of the sound field.

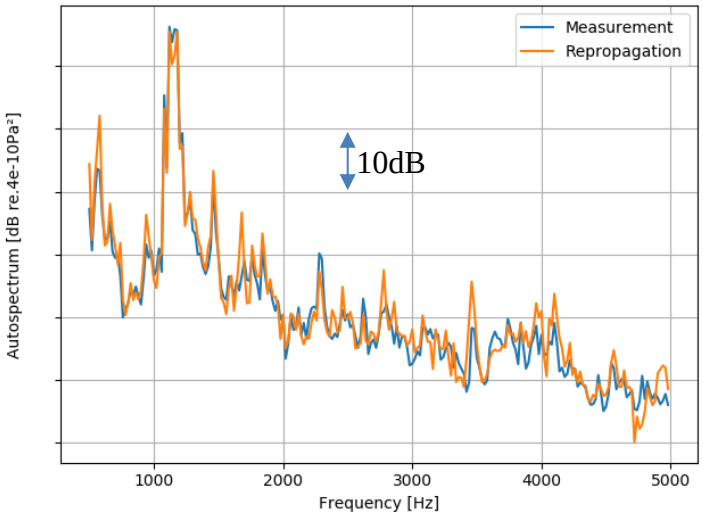

Figure 8: Measured (ground truth) and re-propagated autospectra on the 2nd microphone of the right control array (in black in the Figure 6). The absolute values have been voluntarily masked for the sake of confidentiality

Once the validation has been done, one may re-propagate the sound field everywhere around the motor with confidence. For example, the sound field may be computed over a grid arbitrarily

defined, as shown in Figure 9. This kind of spatial representation of the field may be useful for an acoustical optimization perspective.

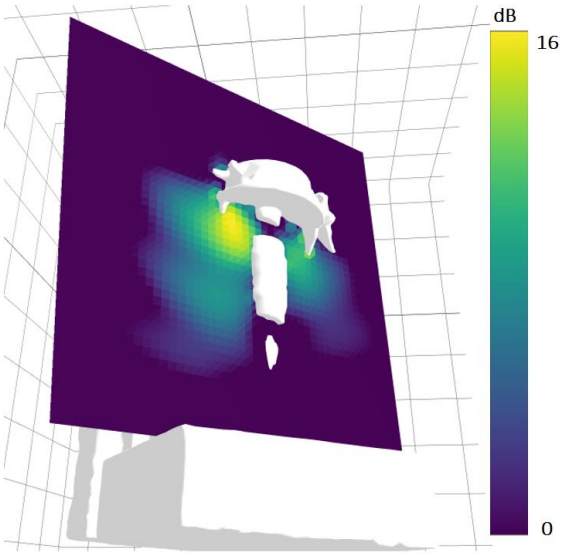

Figure 9: Pressure field re-propagated from identified sources over a grid user-defined at 1150Hz at 1440rpm. The absolute values have been voluntarily masked for sake of confidentiality.

As a remark, it has been observed that the sources produced by the electric motor present in general strong directivity patterns. For this kind of application, inverse methods respecting this behaviour are strongly recommended. The strong directivity of electric machine sources should also be a warning for NVH engineers: unlike for combusting engines, quantification of the global source strength cannot be assessed with only 5 or 6 microphones placed around the motor.

4.3 Run-up application

The process generally applied to characterize the radiation of a motor consists in recording signals during run-up operating condition. Then, by the way of one quick acquisition, all the information is captured by the microphones for the all operating range of the motor. Meanwhile, imaging techniques are generally applied on converged CSM obtained by considering dozens of hundreds snapshots. In this section, iBf will be applied on CSM estimated over one single temporal snapshot to assess the possibility of reconstructing sources during run-up experimental conditions.

Two runs are considered in this section. The first one is measured in stationary conditions at 3940 rpm and the second is measured during a run-up from 500 to 4500 rpm. In the first case, iBf is applied on a CSM computed from 200 snapshots. In the second case, iBf is applied on a CSM computed by considering the snapshot corresponding to the speed of 3940rpm. The Figure 10 presents the autospectrum of one microphone measured during the run-up as a function of frequency and speed. Figure 11 shows the localization maps computed by iBf for the two operating conditions, whereas Figure 10 present the corresponding sound power integrated over the whole mesh.

Finally, the Gibbs sampler presented in [14] has been applied to appreciate the dispersion of the sound power. One thousand samples have been drawn to build the Markov chain. The credible interval has been computed from 0.05 and 0.95 quantiles of a noncentral chi-squared.

The algorithm has not been applied on the run-up measurement since the chain did not converge on non-converged CSM. This result shows the wealth of information that Bayesian approach could provide.

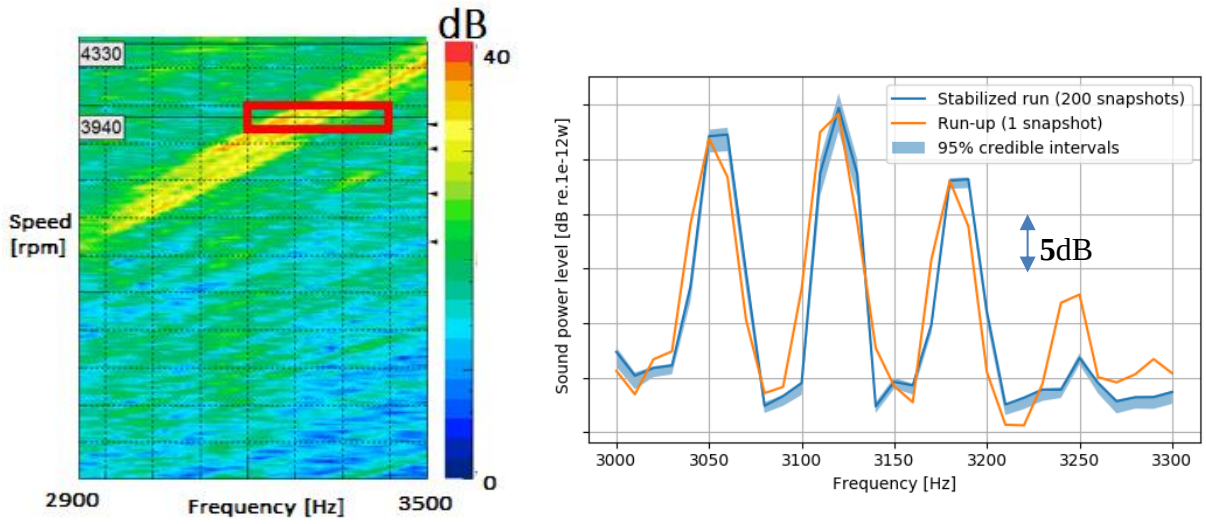

(a) *(b)*

Figure 10: Autospectrum of one microphone recorded during the run-up (a) and sound power spectrum summed on the entire mesh computed by iBf (b) using an averaged CSM (in blue) and instantaneous CSM (in green) at 3940 rpm. The absolute values of the y-axis have been voluntarily masked for sake of confidentiality

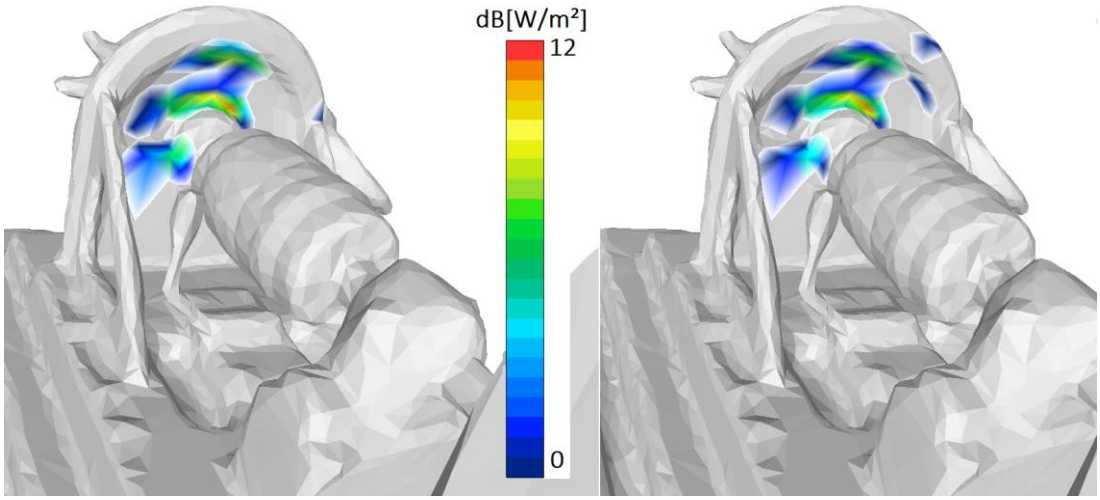

Figure 11: Reconstructed sound power map (around the 48th order) by iBf based on averaged CSM (on the left) and instantaneous CSM (on the right) computed at [3-3.3]kHz (around the 48th order). The absolute values have been voluntarily masked for sake of confidentiality

The similarity of the results demonstrates the robustness of the method regarding the number of snapshots, for this particular application. This robustness is explained by the fact that the regularization parameter adapts itself to the convergence of the CSM. Figure 12 illustrated this

statement. From [23], the relative error of estimation of the CSM may be estimated following this equation:

$$\epsilon[G_{yx}] = \frac{1}{|\gamma_{y:x}|\sqrt{n_d}}, \tag{9}$$

with n_d the number of ensemble average, and $\gamma_{y:x}$ the square root of the coherence between the sensors y and x. Figure 12 presents this quantity averaged over the 90 microphones together with the evolution of the estimation of the regularization parameter computed for an increasing number of snapshots. This curve indicates that the regularization parameter allow the iBf to adapt itself to the convergence of the CSM: if one snapshot is considered, the amount of regularization is larger than if a converged CSM is considered.

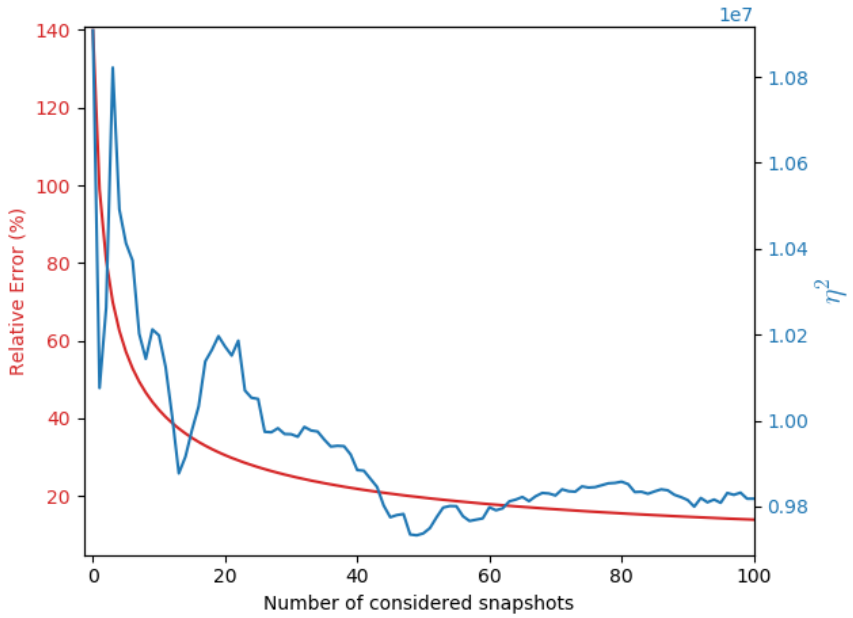

Figure 12: relative error on the cross spectrum estimation and evolution of regularization parameter as a function of number of snapshots for the calculation of the CSM at 3920Hz.

5 CONCLUSIONS

This paper illustrates the application of iBf method on an industrial case. The influence of the quality of the propagation model has been observed. Then, it has been seen that the method respects the directivity pattern of the sources, which can be exploited to design effective acoustic treatment. Finally, the robustness of the method regarding the convergence of the CSM has been assessed. The internal regularization process makes the method more resilient to measurement noise. This observation opens the opportunity to apply the method on run-up operating conditions.

The full characterization process presented in this paper has been experienced on industrial applications and it reveals to be experimentally effective. The installation of the system (digitalization of the motor, setting the position of the array, wiring the cables) takes around half a day. A run-up measurement takes few minutes when the motor is set-up. Then, the post-processing of array signals contains two steps: the calculation of the transfer function by ESM and the application of iBf. The first part requires to place randomly the equivalent source inside

the mesh. An automatic algorithm has been implemented therefore. It has to be executed only once for the full range of frequencies. With an Intel Core i7 CPU (1.8 GHz, 16 Go of RAM) associated with a NVIDIA Quadra K-4100M graphic card, the application of the ESM takes around 6 seconds per frequency when the iBf takes 4 seconds with the considered model (90 microphones, 1000 equivalent sources, 7488 nodes).

6 ACKNOLEDGEMENTS

Authors would like to thank Groupe Renault for allowing us to present these experimental results. This study has been supported by the national project FUI LUG2.

7 REFERENCES

[1] Q. Leclere, A. Pereira, C. Bailly, A. Antoni and C. Picard, “A unified formalism for acoustic imaging,” in *Bebec*, Berlin, 2016.

[2] M.-R. Bai, “Application of BEM (boundary element method)-based acoustic holography to radiation analysis of sound sources with arbitrarily shaped geometries,” *The Journal of the Acoustical Society of America,* p. 533, 1992.

[3] S. Forget, N. Totaro, J.-L. Guyader and M. Schaeffer, “Source fields reconstruction with 3D mapping by means of the virtual acoustic volume concept,” *J. Sound Vib.*, pp. 48-64, 2016.

[4] G. Battista, P. Chiariotti, G. Herold, E. Sarradj and C. P, “Inverse methods for three-dimensional acoustic mapping with a single planar array,” in *Bebec*, Berlin, 2018.

[5] I.-Y. Jeon and J.-G. Ih, “On the holographic reconstruction of vibroacoustic fields using equivalent sources and inverse boundary element method,” *Journal of Acoustical Society of America,* vol. 118 , no. 6, pp. 3473-3482, 2005.

[6] P. Nelson and S. Yoon, “Estimation of acoustic source strength by inverse methods: Part I, conditioning of the inverse problem,” *Journal of sound and vibration,* vol. 233, no. 4, pp. 639--664, 2000.

[7] T. Suzuki, “L1 generalized inverse beam-forming algorithm resolving coherent/incoherent, distributed and multipole sources,” *Journal of Sound and Vibration,* vol. 330, no. 24, pp. 5835-5851, 2011.

[8] T. Le Magueresse and O. Minck, “Source localization inside a cabin using calculated Green's Function,” in *SIA*, Le Mans, 2012.

[9] K. Holland and P. Nelson, “An experimental comparison of the focused beamformer and the inverse method for the characterisation of acoustic sources in ideal and non-ideal acoustic environments,” *Journal of Sound and Vibration* , vol. 331, no. 20, pp. 4425 - 4437, 2012.

[10] J. Antoni, “A Bayesian approach to sound source reconstruction: Optimal basis, regularization, and focusing,” *The Journal of the Acoustical Society of America,* vol. 131, pp. 2873-2890, 2012.

[11] J. Antoni, “A Bayesian approach to sound source reconstruction: Optimal basis, regularization, and focusing,” *The Journal of the Acoustical Society of America,* vol. 131, no. 4, pp. 2873-2890, 2012.

[12] J. Antoni, T. Le Magueresse, Q. Leclère and P. Simard, “Sparse acoustical holography from iterated Bayesian focusing,” *Journal of Sound and Vibration,* vol. 446, pp. 289-325, 2019.

[13] A. Pereira, J. Antoni and Q. Leclère, “Bayesian regularization of the inverse acoustic problem,” *Journal of Sound and Vibration,* 2013.

[14] J. Antoni, C. Vanwynsberghe, T. Le Magueresse, S. Bouley and L. Gilquin, “Mapping uncertainties involved in sound source reconstruction with a cross-spectral-matrix-based Gibbs sampler,” *Journal of Acoustical Society of america,* vol. 146, 2019.

[15] L. B. S. Gilquin, J. Antoni, T. Le Magueresse and C. Marteau, “Sensitivity analysis of two inverse methods: conventional Beamforming and Bayesian focusing,” *Journal of Sound and vibration,* 2019.

[16] G. Koopmann, L. Song and J. Fahnline, “A method for computing acoustic fields based on the principle of wave superposition,” *The Journal of the Acoustical Society of America,* 1989.

[17] H. Cramer, Mathematical Methods of Statistics (PMS-9), Princeton university press, 1999.

[18] A. Pereira, J. Antoni and Q. Leclère, “Empirical Bayesian regularization of the inverse acoustic problem,” *Applied Acoustics ,* vol. 97, pp. 11-29, 2015.

[19] A. Pereira, “Acoustic imaging in enclosed spaces,” 2013.

[20] J. Chambon, T. Le Magueresse and O. Minck, “Three-dimensional beamforming for wind tunnel applications using ESM based transfer functions,” in *Bebec*, Berlin, 2020.

[21] T. Le Magueresse, “Approche multidimensionnelle du problème d'identification acoustique inverse,” Ph. D thesis, Insa de Lyon, 2016.

[22] O. Minck, T. Le Magueresse, L. Lamotte, C. Locqueteau and P. Bouvet, “Array based acoustic power measurement, Renault pass-by noise,” in *Fisita*, 2016.

[23] J. Bendat and A. Piersol, Random data - Analysis and measurement procedures, Wiley, 2010.